BRL

(12)

REPORT NO. 2019

AERODYNAMIC INTERFERENCE DURING SABOT DISCARD

E. M. Schmidt
D. D. Shear

September 1977

USA ARMAMENT RESEARCH AND DEVELOPMENT COMMAND
USA BALLISTIC RESEARCH LABORATORY
ABERDEEN PROVING GROUND, MARYLAND

UNCLASSIFIED

SECURITY CLASSIFICATION OF THIS PAGE (When Data Entered)

REPORT DOCUMENTATION PAGE	READ INSTRUCTIONS BEFORE COMPLETING FORM
1. REPORT NUMBER: ~~BRL Report No. 2019~~ BRL-R-2019	2. GOVT ACCESSION NO. / 3. RECIPIENT'S CATALOG NUMBER
4. TITLE (and Subtitle): AERODYNAMIC INTERFERENCE DURING SABOT DISCARD	5. TYPE OF REPORT & PERIOD COVERED: Final Rept
	6. PERFORMING ORG. REPORT NUMBER
7. AUTHOR(s): E. M. Schmidt, D. D. Shear	8. CONTRACT OR GRANT NUMBER(s)
9. PERFORMING ORGANIZATION NAME AND ADDRESS: U.S. Army Ballistic Research Laboratory, Aberdeen Proving Ground, MD 21005	10. PROGRAM ELEMENT, PROJECT, TASK AREA & WORK UNIT NUMBERS: 1L662603AH78
11. CONTROLLING OFFICE NAME AND ADDRESS: U.S. Army Materiel Development & Readiness Command, 5001 Eisenhower Avenue, Alexandria, Virginia 22333	12. REPORT DATE: SEP 77 / 13. NUMBER OF PAGES: 47 (39 pp)
14. MONITORING AGENCY NAME & ADDRESS (if different from Controlling Office)	15. SECURITY CLASS. (of this report): UNCLASSIFIED
	15a. DECLASSIFICATION/DOWNGRADING SCHEDULE

16. DISTRIBUTION STATEMENT (of this Report)

Approved for public release; distribution unlimited.

DDC RECEIVED FEB 23 1978 B

17. DISTRIBUTION STATEMENT (of the abstract entered in Block 20, if different from Report)

18. SUPPLEMENTARY NOTES

19. KEY WORDS (Continue on reverse side if necessary and identify by block number)

Sabot Discard
Launch Dynamics
Fin-Stabilized Projectiles
Aerodynamic Interference

20. ABSTRACT (Continue on reverse side if necessary and identify by block number) (ner)

An experimental program has been conducted to investigate disturbances to the trajectories of gun-launched, fin-stabilized projectiles during the sabot discard process. Correlated near muzzle and down range measurements of sabot component and projectile motion are acquired using both orthogonal, flash X-rays and a ballistics range. Apparent anomalous yawing motion of projectiles correlates with asymmetries in the sabot discard geometry. The perturbations to the flow around the projectile due to these asymmetries are calculated and shown to be of sufficient magnitude to produce significant alterations in the

DD FORM 1 JAN 73 1473 EDITION OF 1 NOV 68 IS OBSOLETE

050750 1

UNCLASSIFIED

SECURITY CLASSIFICATION OF THIS PAGE (When Data Entered)

desired trajectory. For the rounds tested, the impulse due to aerodynamic interaction during sabot discard is of the same magnitude as the transverse impulse imparted to the projectile during in-bore acceleration.

TABLE OF CONTENTS

LIST OF ILLUSTRATIONS

Preceding Page Bla

I. INTRODUCTION

The primary design being considered for future, anti-armor, kinetic energy rounds is the saboted, fin-stabilized projectile. The presence of the sabot leads to unique problems both in-bore and upon shot exit. Within the gun, consideration must be given to unsupported length of the projectile, fin interactions with the propellant bed, gas sealing between components, and excitation of internal degrees of freedom. At shot ejection, the sabot is discarded, generating a set of mechanical and gasdynamic effects which must be analyzed in order to minimize transverse impulses prior to entry into free flight. Aerodynamic interference between discarding sabot components and the projectile is thought to affect the resultant trajectory; however, to date, measurements have not been obtained to quantify this interference for actual kinetic energy rounds. This report presents the results of an experimental program conducted to examine sabot and projectile dynamics during the discard process. Observations of geometric asymmetry in the sabot discard pattern and associated, anomalous behavior of the projectile are used to postulate the existence of strong aerodynamic interactions.

While aerodynamic interference associated with components of aircraft, e.g., wing-body, airframe-propulsion, and airframe-stores, has been extensively investigated[1], similar interference associated with sabot discard from high speed projectiles has received limited attention[2-4]. Gallagher[2] presents an experimental investigation of projectile deviation from the desired aim point due to muzzle blast, sabot discard, and projectile asymmetry. Since he neglects any contribution due to gun tube/projectile interaction, the value he assigns to

---

1. *Sears, W. R., ed., "Aerodynamic Interference," AGARD, CP-71-71, January 1971.*

2. *Gallagher, W. J., "Elements which have Contributed to Dispersion in the 90/40mm Projectile," Ballistic Research Laboratory Report No. 1013, March 1957, AD 135306.*

3. *Conn, H., "The Influence of Sabot Separation on the Yawing Motion of a Cone," Defense Research Establishment, Valcartier, Canada, TN 1849/70, June 1970, AD 880697L.*

4. *Glauz, W. D., "Estimation of Forces on a Flechette Resulting from a Shock Wave," Midwest Research Institute, Kansas City, MO, Final Report 19 June 1970 - 18 March 1971, May 1971. AD 724178.*

deviation due to muzzle blast is orders of magnitude greater than that found in more recent investigations[5,6] which show that muzzle blast does not contribute significantly to trajectory deviation and that the actual source lies with gun tube or sabot discard interactions. Gallagher notes that the sabot components open symmetrically, but the center of gravity of the grouped components does not lie along the axis of the projectile. He assumes that there will be a momentum exchange between the sabot and projectile in relation to their masses and the magnitude of the center of gravity separation. However, due to the limitations of his apparatus, Gallagher could not define the magnitude of this deviation which is generated by elastic rebound at muzzle ejection. Gallagher made no attempt to investigate the effects of aerodynamic interactions.

Conn[3] investigates the effect of aerodynamic interference between sabots and projectiles fired from a light gas gun. His measurements show that a conical projectile launched with a two-segment sabot has periods of pitch and yaw which are dependent upon the orientation of the sabot plane of separation. He uses oblique shock and Newtonian flow theory to analyze the pressure distribution on a cone at arbitrary attitude relative to a symmetrically discarded, two-segment sabot. The results of his analysis show that aerodynamic interference differentially increases the restoring moments acting on the cone, thereby shortening the periods of oscillation. He notes that by intercepting the sabot components at the extremum point of projectile yaw, the free flight yaw levels are minimized.

Glauz[4] uses oblique shock theory to analyze the side forces and moments generated on a fin-stabilized projectile due to a single sabot component flying in close proximity. He assumes that when it intercepts the projectile, the shock wave from the sabot is planar, does not reflect at the projectile, and is not influenced by the projectile viscous or inviscid flow field. In a sample calculation, Glauz predicts a significant alteration of the trajectory of a small caliber flechette by this type discard process; however, his calculated value of discard induced angular velocity is an order of magnitude higher than actually measured[7]. This disagreement is due to both the simplistic nature of the model and the complex, mutually interacting flows established during discard.

---

5. *Gretler, W., "Intermediate Ballistics Investigations of Wing Stabilized Projectiles," Deutschen Versuchsanstaldt fur Luft-und Raumfahrt, Aachen, Germany, R67-92, November 1967.*

6. *Schmidt, E. M., Fansler, K. S., and Shear, D. D., "Trajectory Perturbations of Fin-Stabilized Projectiles due to Muzzle Blast," Journal of Spacecraft and Rockets, Vol 14, June 1977, pp. 339-344.*

7. *Schmidt, E. M. and Shear, D. D., "Launch Dynamics of a Single Flechette Round," Ballistic Research Laboratory Report No. 1810, August 1975, AD B006781L.*

The present investigation was conducted to provide detailed information on the aerodynamic interference between sabot components and projectiles for actual kinetic energy round configurations. The results of measurements of sabot and projectile motion from the muzzle, through sabot discard, and into free flight are presented. Observed variations in projectile angular motion is shown to correlate with measured sabot discard asymmetry. A simple model of the interacting flow is used to estimate the projectile behavior. Like previous models, the agreement is not exact; however, the results do support the interpretation as to the cause of anomalous projectile angular motion.

II. DATA ACQUISITION AND REDUCTION

The test projectile, Figure 1, has a body diameter of 23mm, a length of 423mm, and is stabilized by four fins having a width of 56mm. A four segment sabot is employed to launch the round from a 60mm gun. The launch velocity is 1310 m/s, and since the gun tube has a twist of one turn in 200 calibers, the projectile enters free flight with a roll rate of 110 revolutions per second. The projectile launch and flight dynamics are measured using a variety of techniques, Figure 2.

Near muzzle motion is monitored at six, orthogonal X-ray stations located at 1.7m intervals over the first 9.0m of the trajectory. The X-ray photographs provide information on the sabot and projectile motion through the muzzle blast and during sabot discard. Located downrange of the X-ray stations, five smear cameras set at 4.6m intervals provide coverage of the final, aerodynamic discard of the sabot components. These components are intercepted at an armor plate shield, and the projectile enters the BRL Transonic Range. This range consists of an array of 25 orthogonal, spark shadowgraph stations extending over 180m of the projectile trajectory. The detailed free flight motion of the round is measured as it traverses the Transonic Range and is used for two purposes. First, it provides a basis for the determination of the aerodynamics of the projectile:

$$C_{L_\alpha} = 10.1,$$

$$C_{M_\alpha} = -21.5,$$

$$C_D = 0.461.$$

Second, the least squares fit to the projectile yawing motion through the range is extrapolated back into the region where X-ray data is acquired. This permits comparison of the two sets of measurements.

To permit rapid, quantitative reduction of the X-ray data, an *in situ* calibration procedure is employed. The technique is straightforward; consisting of surveying a calibrated steel wire into position

along the line of fire, taking X-ray photographs of the wire just prior to the shot, removing the wire, and firing the test. In this manner, a double exposure is obtained at each X-ray station, Figure 3. On this photograph, the wire with known spatial location, and the projectile, whose properties we wish to measure, are clearly visible. The reduction of the data on the film is direct for objects located near the calibration wire, i.e., the projectile. Determination of the location and orientation of objects distant from the wire, i.e., sabot components, requires correction for parallax.

The X-ray units used are Field Emmission Corporation, Flexitron Model 730/2722 (180KV) and 730/2235 (150 KV) Pulsed X-Ray Systems.* Two separate triggering systems are employed, Figure 4. The first, located near the muzzle, triggers the delay units for the X-ray stations located at 0.6, 2.3 and 4.0m from the gun. The arrival of the muzzle blast wave at an externally mounted, piezoelectric transducer is used as a definitive indicator of shot ejection; however, it is necessary to eliminate the danger of triggering from spurious signals generated during the firing process (e.g., due to the high voltage electric primer, propellant ignition and pressurization, gun tube vibration, precursor blast, Figure 5). This is accomplished through the construction of a trigger logic sequence which senses both the arrival of the precursor blast, caused by ejection of the tube air ahead of the projectile, and the main, propellant gas-generated blast. A Tektronix Type 555, Dual Time Base Oscilloscope is used in conjunction with a laser beam and the muzzle mounted pressure transducer, Figure 4. The laser beam is passed close to the muzzle of the gun and is deflected by the arrival of the precursor blast. This is sensed on a photomiltiplier whose output triggers the first time base of the oscilloscope. After a delay of sufficient duration to permit the precursor blast to pass over the pressure transducer, the second time base of the oscilloscope is enabled or cocked. This time base is set to trigger upon the arrival of the next pressure pulse sensed by the transducer, the main muzzle blast, and provides the trigger pulse to the X-ray delay units.

The second trigger system controls the X-ray units located at 5.8, 7.4, and 9.0m from the gun. As indicated in Figure 4, this system is simply a double pass, laser light beam. Since the projectile penetrates the muzzle blast at a distance of 1.5m from the gun, there is no danger of pretriggering these stations. The dual trigger systems are employed to eliminate the need for long delay inputs to the X-ray units and to provide redundancy in case of failure.

The reduction of the X-ray data, at least as far as determining the projectile motion, is relatively simple. The position of the projectile center of gravity and the orientation of its axis of symmetry are measured with respect to the calibration wire and fiducial beads strung

Use of trade names does not constitute indorsement by the Government.

upon it, Figure 3. These measurements are corrected for the wire catenary, the viewing plane of the X-ray film, and the c.g. trajectory[7]. Final presentation of the data is made in a coordinate system identical to that used in the Transonic Range reduction, Figure 6. In this system, β is the angle of sideslip (measured positive as shown) and is the angle between the projectile velocity vector and the plane containing the projectile axis and a vector parallel to the Y-axis. The angle of attack, α, is the angle between the normal projection of the velocity vector into the aforementioned plane and the projectile axis.

III. EXPERIMENTAL RESULTS

Ten rounds were fired in this test series. Transonic Range data was acquired on all ten; however, full X-ray coverage was obtained on only eight of these. The Transonic Range data and its extrapolation back to the muzzle gives a direct indication of the impact of sabot discard interactions upon the projectile dynamics, Figure 7. For clarity, only five of the ten rounds are plotted; however, all ten rounds are summarized in Table 1, below. The weapon muzzle is located at Z=0; thus, the extrapolation shows yaw levels at this point well in excess of expected in-bore values of less than 0.1^{o}. Further, while the period of yaw (distance between successive maxima or minima) is relatively stable, the location of the first maximum yaw varies considerably.

Round No.	Muzzle Yaw (degrees)	First Max. Yaw (degr.)	$Z_{1st\ Max.}$ (m)	L, Yaw Period (m)
1	1.8	3.31	27.5	40.8
2	2.2	6.52	24.0	40.6
3	4.2	7.78	26.5	39.8
4	0.4	1.74	16.0	36.3
5	1.4	3.68	22.3	37.0
6	1.9	3.02	11.3	38.3
7	3.3	4.29	29.0	38.7
8	3.1	4.45	10.5	39.8
9	3.8	5.59	28.9	40.0
10	2.8	8.07	23.8	40.4

Table 1. Summary of Projectile Yawing Motion from Transonic Range Data.

The period of yaw varies from a minimum of 36.3m to a maximum of 40.8m with a one-sigma standard deviation of 1.5m. Since the period of yaw of a statically stable projectile may be approximated as

$$L = 2\pi \left[2I_y/C_{M_\alpha} \rho A \ell\right]^{\frac{1}{2}}, \quad (1)$$

the consistency of the measured values of L shows that the inertial and aerodynamic properties of the in-flight projectiles are similar for all firings.

In contrast, the location of first maximum yaw varies strongly, covering a range of 10.5 to 29.0m from the muzzle with a one-sigma standard deviation of 7.0m. This dispersion of peak yaw location in combination with the regularity of yaw period explains the failure of the extrapolated range data to produce a minimum yaw point at the muzzle. The cause of this dispersion is interactions between the projectile and discarding sabot components. To visualize this point, consider the yawing motion of a spin stabilized projectile. The round leaves the weapon with small yaw, but finite yawing velocity; subsequently, the yaw grows monotonically until a first maximum yaw is reached at a distance from the muzzle equal to one-half the period of yaw. This behavior is observed in range measurements and is indicative of the round experiencing free flight, aerodynamic loads immediately following ejection. Since the current test projectile has first maximum yaw locations greatly in excess of a reasonable distribution (e.g., 0.75m) about the half-period location 19.6m, it is apparently experiencing an initial environment significantly different than undisturbed free flight.

The X-ray data provides information on the nature of these launch disturbances, Figure 8. This sequence of photographs is compiled from the vertical plates of each of the six, X-ray stations exposed during a single firing. The film plane is parallel to the ground and above the flight path, Figure 4; therefore, the view is that of an observer situated above the projectile watching it fly downrange beneath him. The stations are located over the first 9.0m of the trajectory. The sabot components remain in close proximity to the projectile through the X-ray range; however, by the first smear camera, located 13.7m forward of the gun, Figure 9, they have achieved sufficient lateral and rearward separation to preclude communication with the projectile. It is estimated that interaction between the sabot and projectile flowfields terminates at approximately 11.0m from the muzzle. Interestingly, 10.5m is the smallest Z_{1st} Max. from Table 1; while 29.0m is the largest value. The former value corresponds well to the termination of the interaction zone, and the latter is nearly equal to the sum of this distance and the half period of yaw.

Examination of the discard sequence reveals some interesting features, Figure 8. At the first X-ray station, the only observable motion of the sabot is the shedding of plastic centering and obturating

bands. At 2.3m, the sabot components have moved laterally away from the projectile but show little pitch or yaw. This initial motion is thought to be due to a combination of elastic decompression at separation and the tangential/angular velocity due to the launch roll rate (110 rev/s), and is carried through the muzzle blast with very little amplification. The round penetrates the muzzle blast at approximately 1.5m. Once out of the blast, strong aerodynamic loadings will be generated on the sabot components (launch Mach number - 3.91). The effect of these loads is not seen at 2.3m, but by the third X-ray station, Z=4.0m, the components are pitching away from the projectile due to loads on the front chamfer of the sabot. Subsequent X-ray photographs show the continuation of this pitching motion and resultant lifting away from the projectile. Due to the high drag of the light, sabot components at this attitude, they are decelerated more rapidly than the projectile and fall behind relative to the flight body.

In the final two photographs of this sequence, an asymmetry in the discard geometry is apparent. The sabot petal on the left side (upper component in picture) is closer to the projectile than is the right hand petal. A construction of the sabot pattern at Z=7.4m clarifies this asymmetry, Figure 10. The view is from the rear along the axis of the projectile at cut A-A, Figure 8e. While the photograph appears to show possible contact with the fins, the construction shows that this is not the case. The upper and lower sabot components are symmetrically arranged with respect to the projectile; however, this is not true of the lateral components. The left component is extremely close to a fin surface, suggesting the probability of strong interaction between the two flow fields.

The measured yawing motion gives an indication of the magnitude of aerodynamic interference. A plot of the projectile angles of attack and sideslip for five typical firings is presented in Figure 11. Each data point is a separate measurement from an orthogonal X-ray station. The data is presented as if one were viewing the projectile from the rear; effectively, the coordinate axes could be thought of as representing the fins while the data point corresponds to the attitude of the projectile nose relative to them. A variety of yawing motions are observed. All start with a magnitude of yaw near the muzzle which is quite small, roughly 0.1^{o}, and consistent with anticipated in-bore values. These contrast with the range extrapolations given in Table 1 indicating the error in attempting to carry the Transonic Range data fit through the sabot discard region. The angular velocities at the muzzle are significant and have fairly random orientations. Some rounds show a monotonically increasing yaw, while others have yaw which first increases to a maximum value quite close to the gun and then begins to decrease. It should be remembered that these data are taken over the first 9.0m of flight and are well inside the nominal first maximum yaw location on the trajectory, i.e., half period point at 19.5m.

A comparison of the photographs of Figure 8 with the measured yawing motion of Round 9 presented in Figure 11 correlates the anticipated aerodynamic loads and the observed projectile dynamics. Since the left hand sabot petal is close to the fins while its opposite partner is quite remote, the cross flow generated on the fin surface by the proximity of this petal would create an unbalanced force on the fin directed to the right. In turn this force would cause the projectile nose to yaw left. This is exactly the motion measured in the X-ray data, Figure 11. The angular acceleration produced by this interaction is substantial, $\ddot{\beta} = 0.72 \times 10^4$ rad/s^2. It is reasonable to attempt a determination of the possibility of aerodynamic loadings generating such acceleration.

A simple upper bound model of the interference loadings can be obtained by considering the flow configuration shown in Figure 12. The sabot component is approximated as a semi-infinite, two-dimensional wedge. The wedge angle is taken as 30°, an average of the inclinations of the cylindrical and ramp portions of the sabot relative to the projectile. From the two dimensional shock relations[8], the change in properties for a free-stream flow of $M_\infty = 3.91$ being deflected through 30° are

$$p_2/p_\infty = 8.92,$$

$$M_2 = 1.80.$$

This shocked flow impinges on the fin surfaces and is deflected back to the axial direction. At $M_2 = 1.80$, the flow deflection angle of 30° is in excess of that possible for an attached shock. The calculation of flow with detached shocks is too complex for this approximation; therefore, it is assumed that the flow stagnates on the fin surfaces after passing through a normal shock. For

$$M_2 = 1.80,$$

$$p_{t_3}/p_2 = 4.67,$$

and the pressure on the fin surface is

$$p_{t_3}/p_\infty = 41.6.$$

From the known fin area, c.g. location, and moment of inertia, the

---

8. *Ames Research Staff, "Equations, Tables, and Charts for Compressible Flow," NACA 1135, 1953.*

angular acceleration is calculated

$$\ddot{\beta} \text{ calc.} = 9.7 \times 10^4 \text{ rad/s}^2.$$

This value is a full order of magnitude greater than the measured angular acceleration, indicating that the measured alterations in projectile dynamics are well within the upper bound of this crude model; i.e., they are due to aerodynamic interference.

While in Figure 11 the rounds showing the most obvious effects of aerodynamic interactions are Rounds 7 and 9, the variation in $Z_{1st\ Max.}$, Table 1, points out that all are experiencing sabot launch related disturbances. Not all the observed interactions are detrimental, e.g., Round 8. It leaves the gun with the highest measured launch velocity; however, the initial rate is opposed by the interaction moment which nearly nullifies it by the last two stations. Since the sabot interference ceases approximately two meters farther downrange, it would be expected that the projectile, having a finite yaw angle but nearly zero yaw rate, would effectively enter free flight at a maximum yaw point in its trajectory. Comparison of the X-ray data and the Transonic Range extrapolation shows that this is in fact the case, Figure 13. Both sets of data agree in predicting both the magnitude and rate of change of yaw at roughly 10m from the gun. Closer than this distance, they are in disagreement as would be expected.

A further indication of the agreement between the X-ray and Transonic Range data is provided in Figure 14. This plot shows the yawing motion for Round 9. It is observed that initially, the X-ray data predicts a yawing motion which is opposite to the range extrapolation; however, inclusion of the final two stations shows that the effect of aerodynamic interaction is to reverse this initial angular rate and bring the two sets of data into consistency as to the prediction of the initial free flight motion of the projectile. The other rounds fired compare equally well indicating the validity of the X-ray measurements and supporting the conclusion that strong aerodynamic interference between the sabot and projectile flowfields is occurring.

The impact of interference upon the projectile trajectory can be seen by considering the change in the projectile angular rate during the discard process. Two sources of information are available. The first is the X-ray measurements obtained at the first three stations. Using a differencing formula, ξ_2, the angular rate at Station 2, Z = 2.3m, may be evaluated. This rate is equivalent to the impulse transferred to the projectile during its in-bore acceleration and through the muzzle blast, i.e.,

$$M = I \ddot{\xi} \qquad (2)$$

and

$$\dot{\xi} = \int_0^{\tau} (M/I)dt \approx \text{Angular impulse} \qquad (3)$$

where τ = arbitrary time of interest. The second source of information is provided by Transonic Range data. From the measured value of first maximum yaw, the effective "launch" angular velocity may be evaluated. Neglecting spin and damping terms,

$$\dot{\xi}_o = \xi_{1st\ Max.} \left(C_{M_\alpha} \rho V^2 \ell A/2I_y\right)^{\frac{1}{2}} \qquad (4)$$

The rate given by Equation (4) represents the cummulative angular impulse transferred to the projectile by in-bore, muzzle blast, and sabot discard loadings. Following this reasoning, the difference of these two rates should give the impulse due aerodynamic interference:

$$\Delta\dot{\xi} = \dot{\xi}_o - \dot{\xi}_2 \qquad (5)$$

= change in angular velocity due to discard loads.

These impulse parameters are compared in Table 2.

Round No.	$\lvert\dot{\xi}_2\rvert$ (°/s)	$\lvert\dot{\xi}_o\rvert$ (°/s)	$\lvert\dot{\xi}_2\rvert - \lvert\dot{\xi}_o\rvert$ (°/s)
1	no X-ray	354	-
2	365	686	321
3	239	827	588
4	174	186	12
5	205	393	188
6	427	323	-104
7	98	459	361
8	818	481	-337
9	74	592	518
10	342	862	520

Table 2. Comparison of Angular Velocities (Impulse)

While the last column is a scalar rather than vector difference, it does indicate the relative magnitude of the impulse generated by aerodynamic interaction. Comparison of the last column with the second column shows that the aerodynamic interaction effect is equivalent to that due to in-bore and muzzle blast loadings. This has a significant impact upon accuracy. The impact distribution of the various rounds on-target are computed using two procedures: 1) extrapolation of X-ray Station 2 dynamics downrange through use of the jump relations, and 2) from measured projectile position at the final Transonic Range station. These are presented in Figure 15. Both of the procedures yield elliptical impact patterns with identical orientation of the principal axis; however, there are differences in the size of the patterns. As expected, the extrapolated X-ray data presents the smallest pattern since it does not include the effect of aerodynamic interactions. The measured impact pattern is roughly 30% greater in area than is the extrapolated pattern. This difference indicates that the growth of dispersion due to aerodynamic interference between the sabot components and the projectile is significant in terms of the overall system accuracy.

An unresolved question is the origin of the asymmetries in the sabot discard pattern. It is likely that the interior ballistics and mechanical disengagement of the round have an important input in generating the initial separation dynamics which drive the generation of sabot pattern asymmetry. Additionally, it has been conjectured that differential fracture of the front and rear bands could be a contributing factor. At present, it appears that the best solution to the problem of decreasing the effect of interference lies not in reducing asymmetry, but in providng for more rapid discard. Increasing the speed with which the sabot clears the projectile will decrease the impulse transferred due to asymmetries.

IV. CONCLUSIONS

An experimental program is presented which defines the sabot discard and launch dynamics of a 60mm, fin-stabilized projectile. The resulting data indicate that aerodynamic interference occurs between the discarding sabot components and the projectile. A simple analysis of the magnitude of aerodynamic loadings that could be generated in the discard process indicates that the measured alterations of the projectile trajectory are well within the analytical upper bound. The impulse due to interaction is found to be of the same magnitude as the in-bore and muzzle blast impulse. Its effect is to increase the dispersion of the system significantly. To reduce the impact of aerodynamic interaction, it is advisable to implement rapid sabot discard thereby decreasing the duration of impulse loadings.

ACKNOWLEDGMENTS

The authors were dependent upon Messrs. William Thompson and Donald McClellan for their efforts in the acquisition of the data presented in this report and Messrs. James Bradley and James Carduff for their assistance in the reduction of the Transonic Range Data.

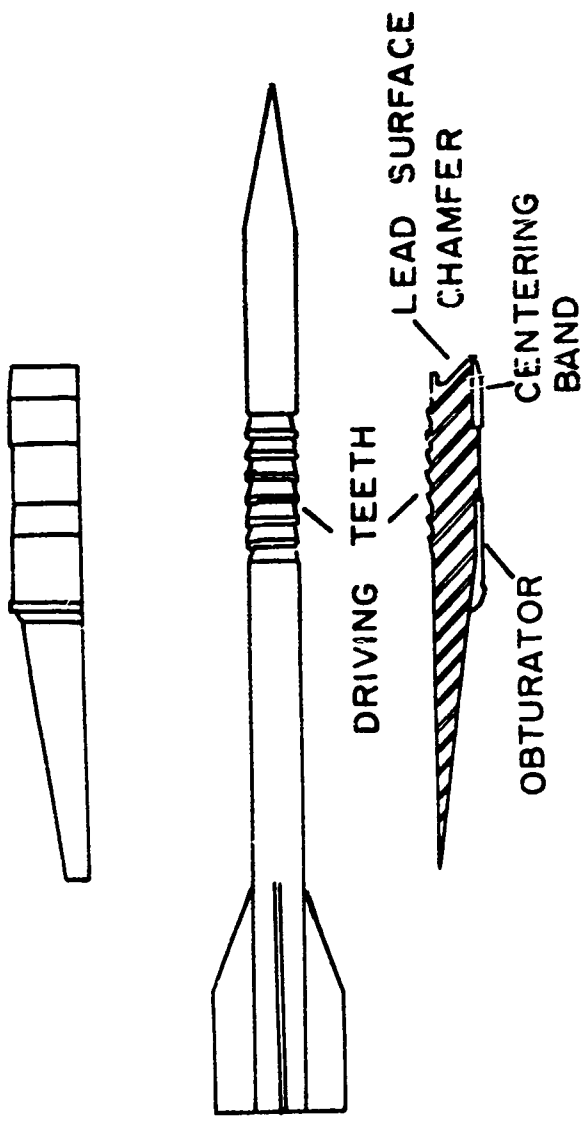

Figure 1. Test Projectile (60mm, AAAC)

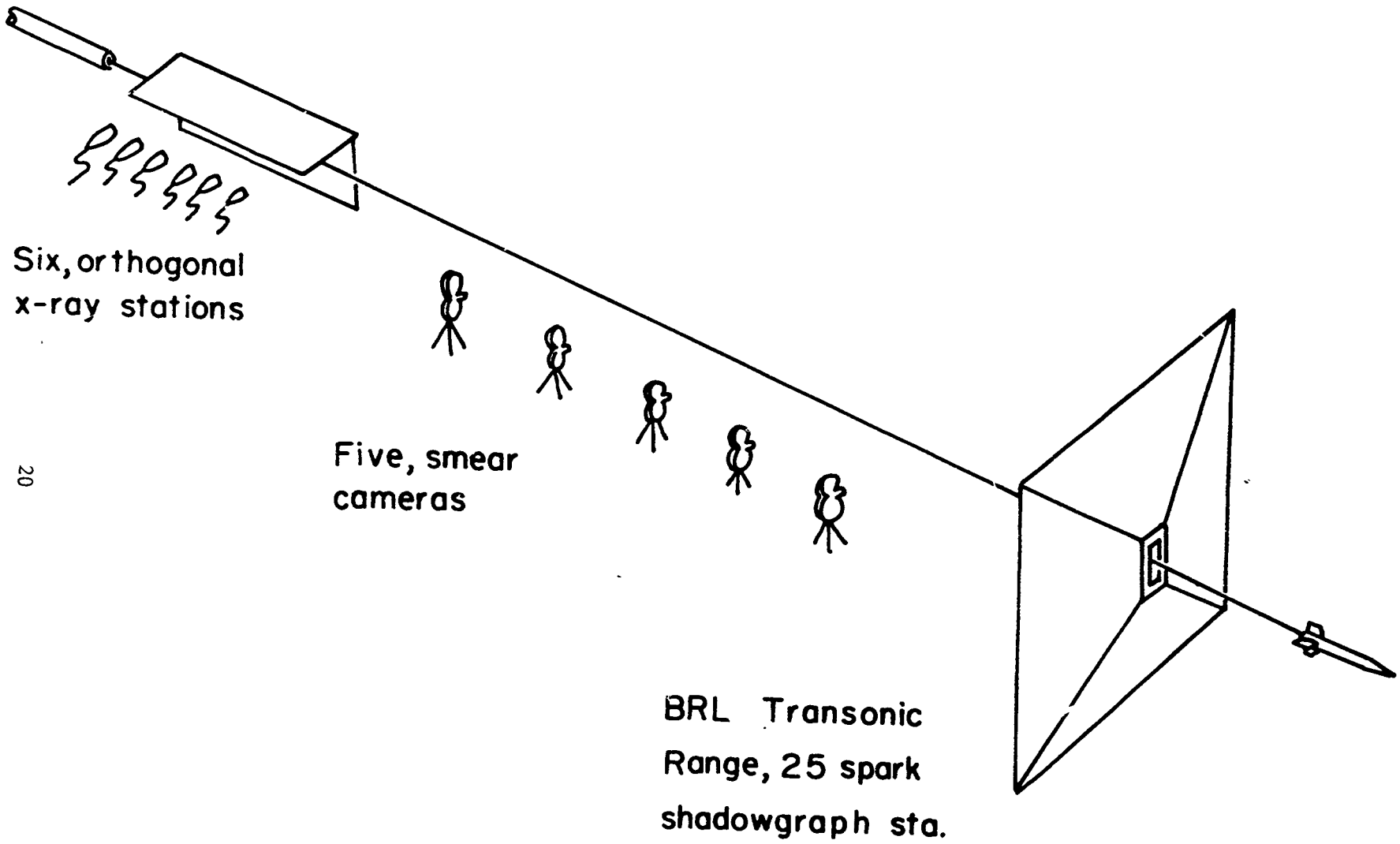

Figure 2. Schematic of Test Set-Up

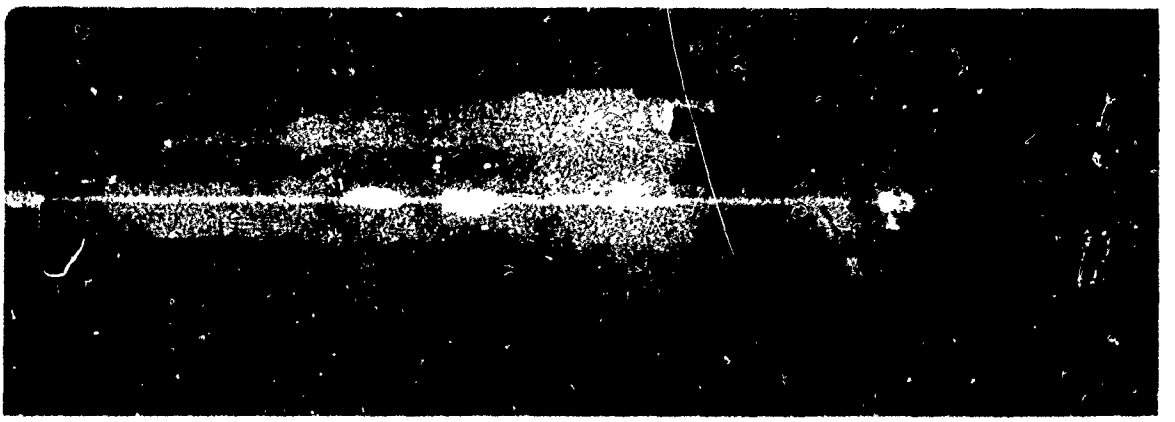

Figure 3. Sample X-Ray Exposure

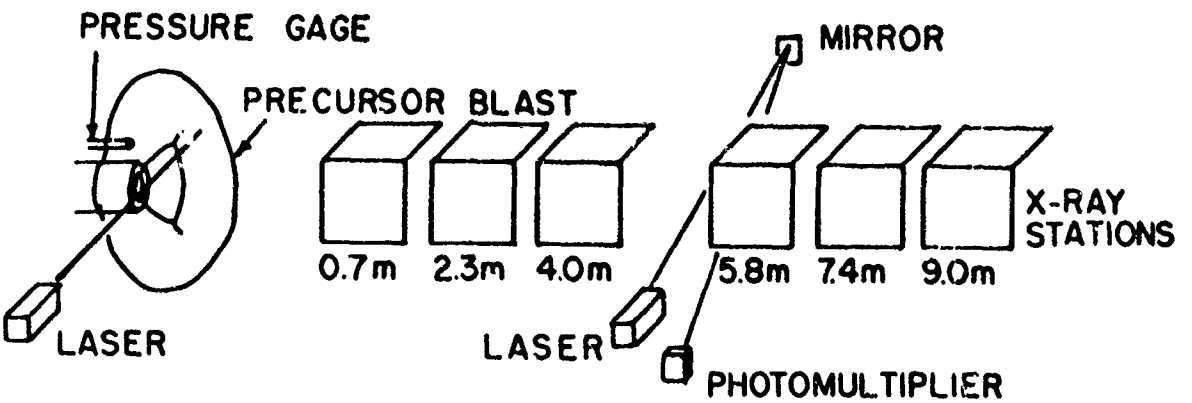

Figure 4. Schematic of Triggering Arrangement

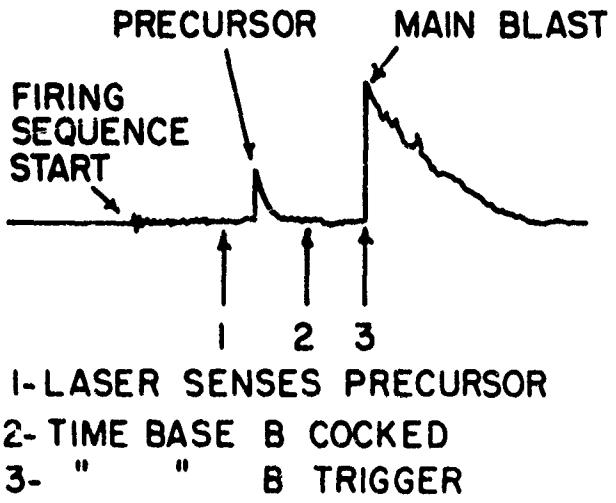

Figure 5. Sample Pressure Trace

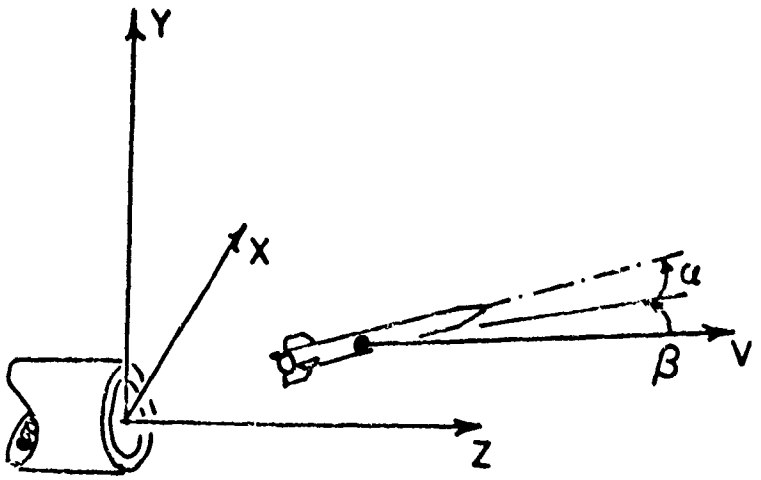

Figure 6. Coordinate System

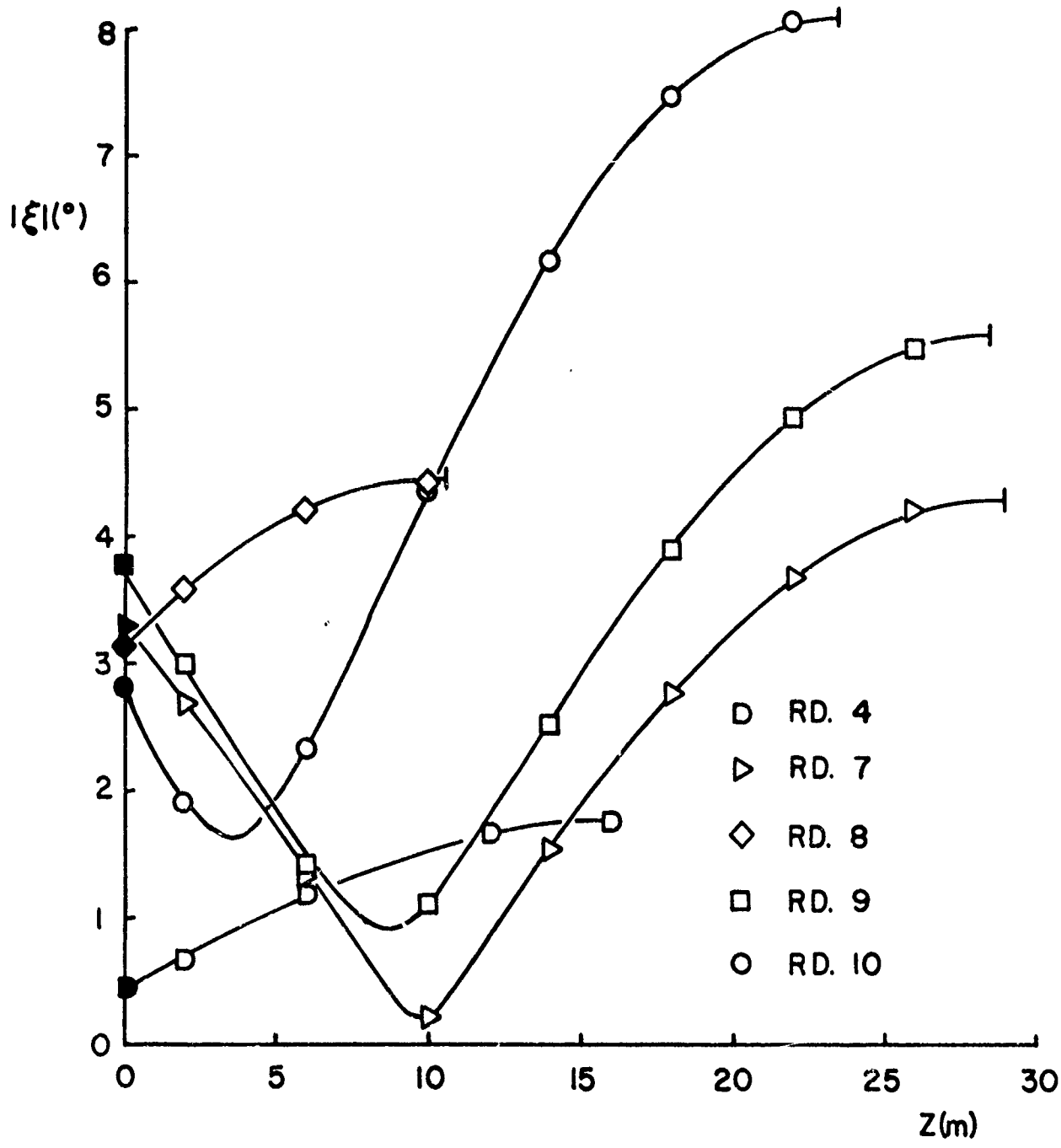

Figure 7. Extrapolation of Transonic Range Data Fit (Darkened symbols represent muzzle location and bars represent first maximum yaw location)

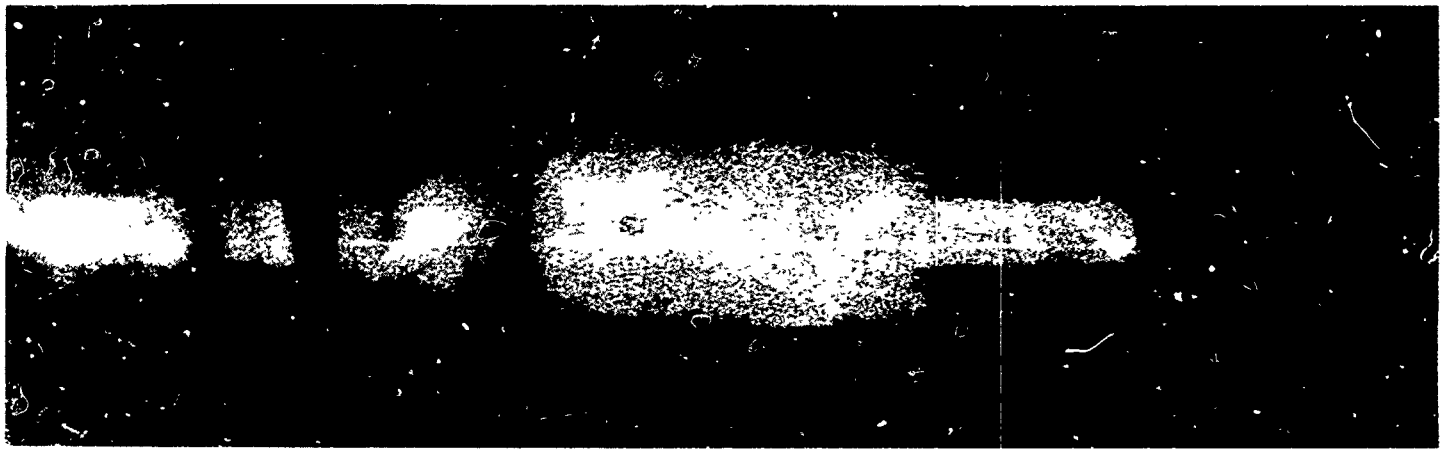

Figure 8. X-Ray Photograph Sequence, Vertical Plates, Round 9.
a. Z = 0.7m

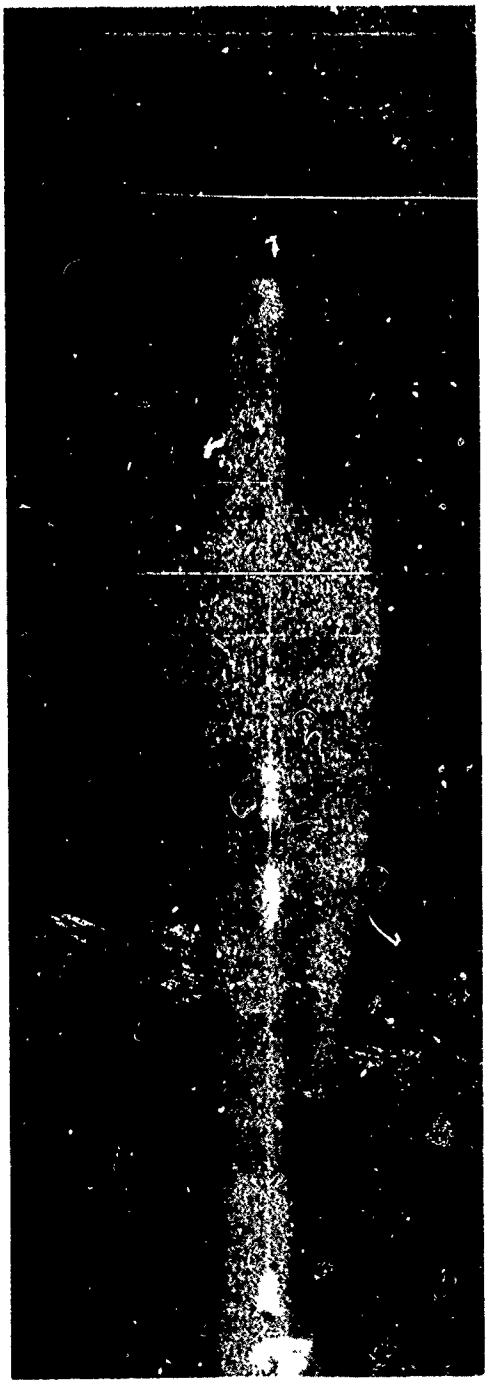

Figure 8b. Z = 2.3m

Figure 8c. Z = 4.0m

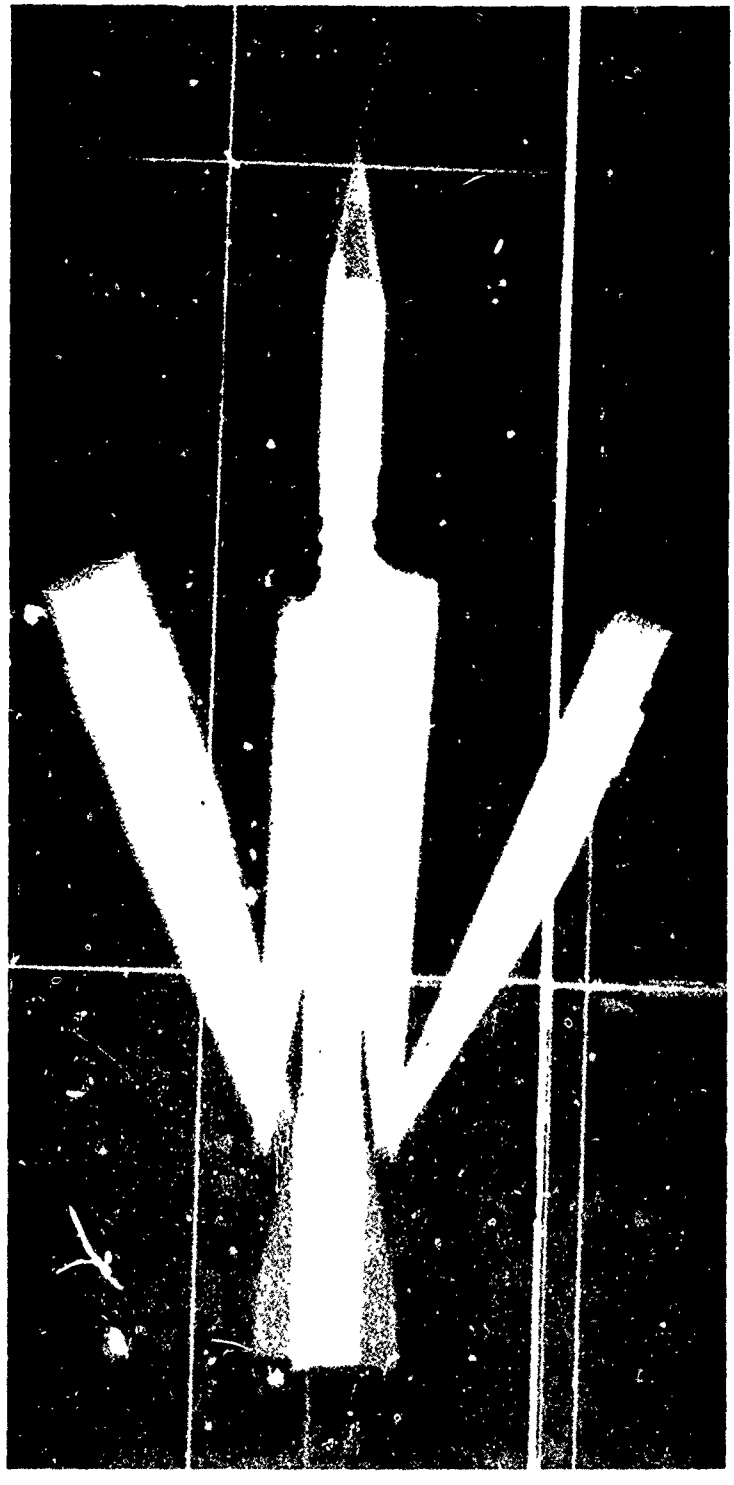

Figure 8d. Z = 5.8m

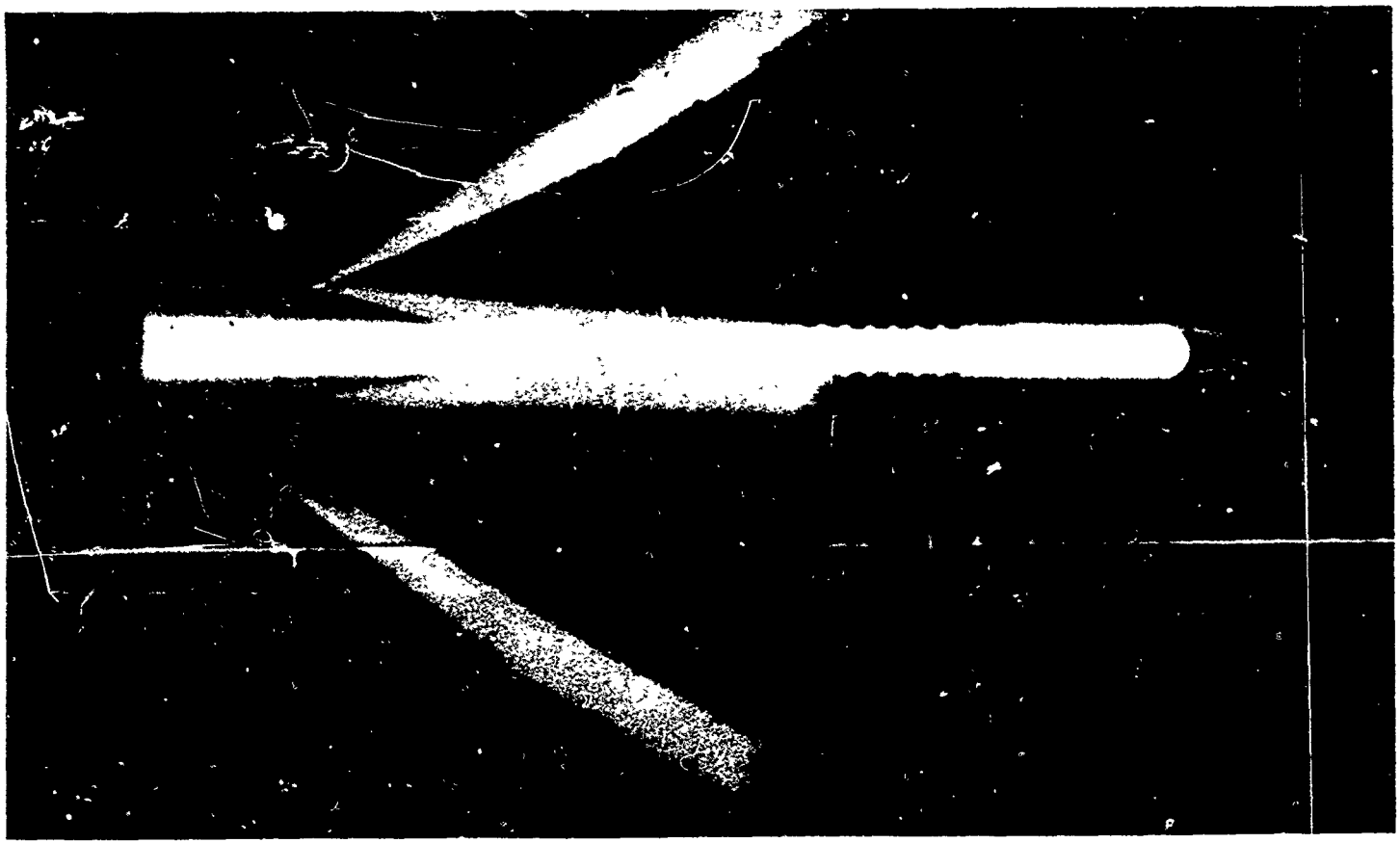

Figure 8e. Z = 7.4m

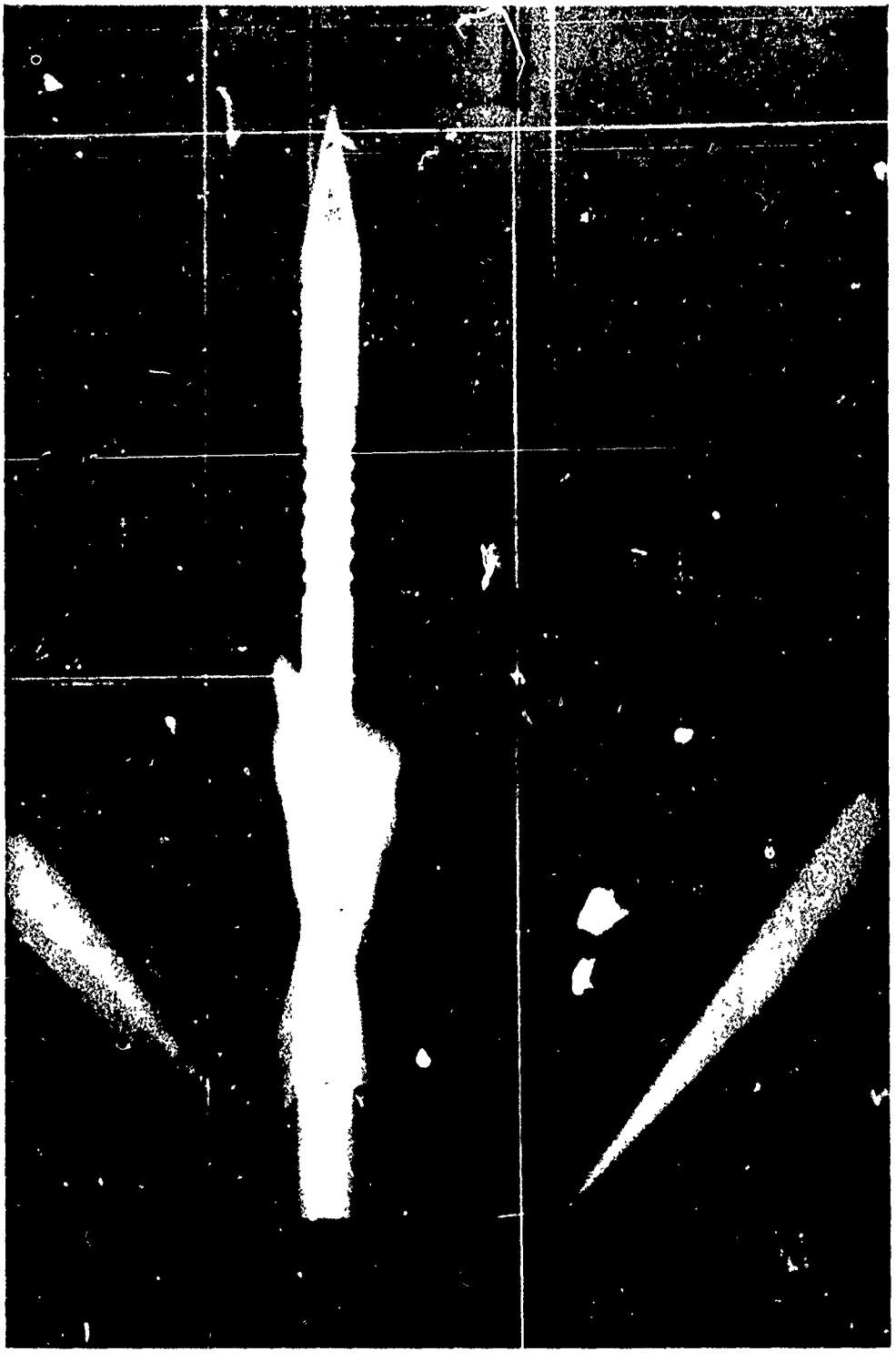

Figure 8f. Z = 9.0m

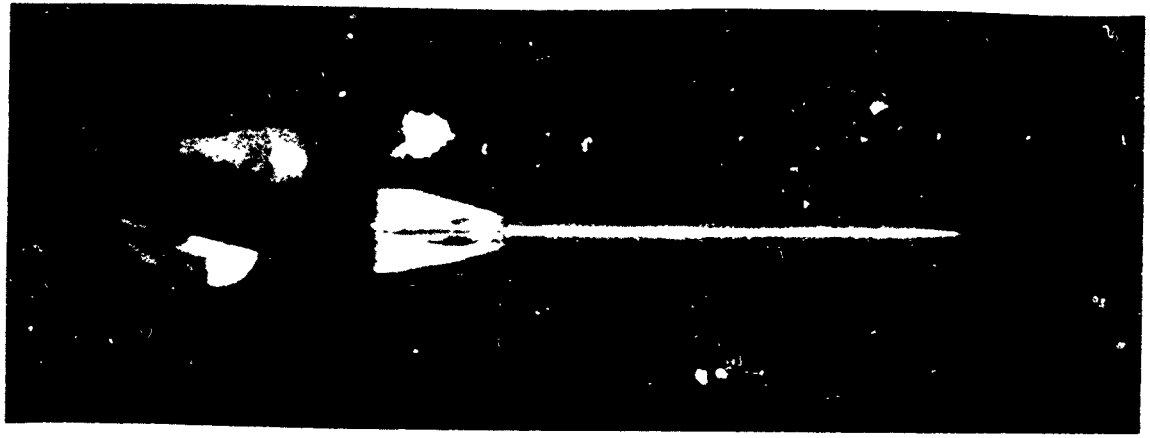

Figure 9. Smear Camera Photograph, Z = 13.7m

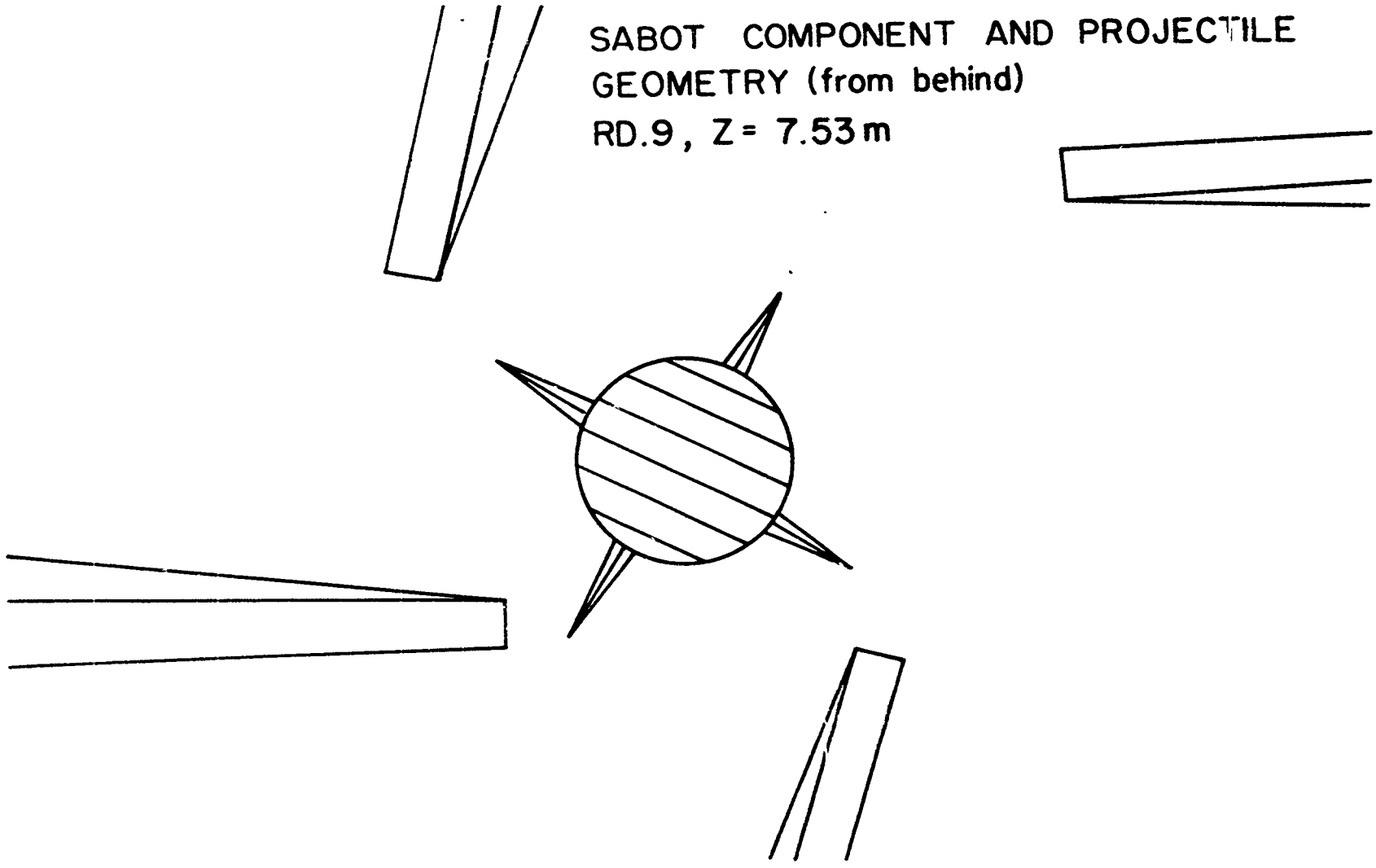

Figure 10. Sabot Pattern, Round 9

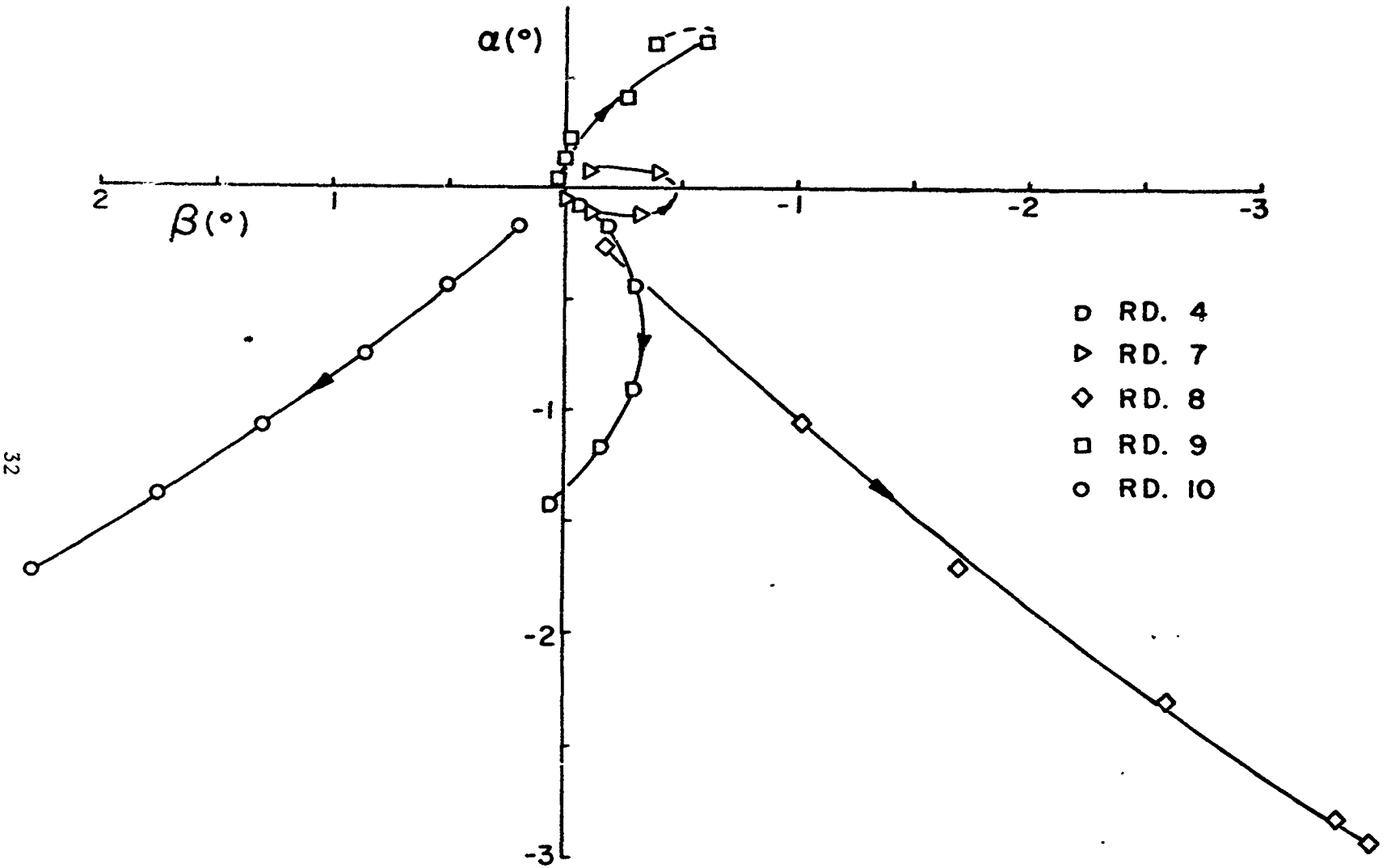

Figure 11. Projectile Yawing Motion Measured From X-Rays

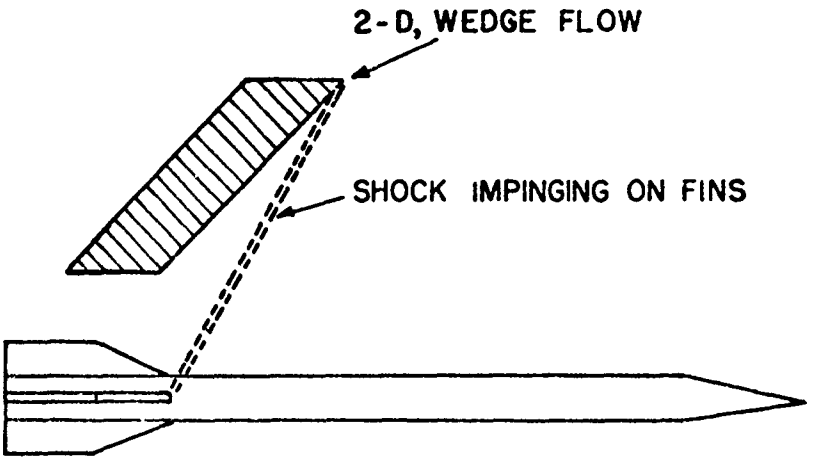

Figure 12. Flow Configuration for Upper Bound Model

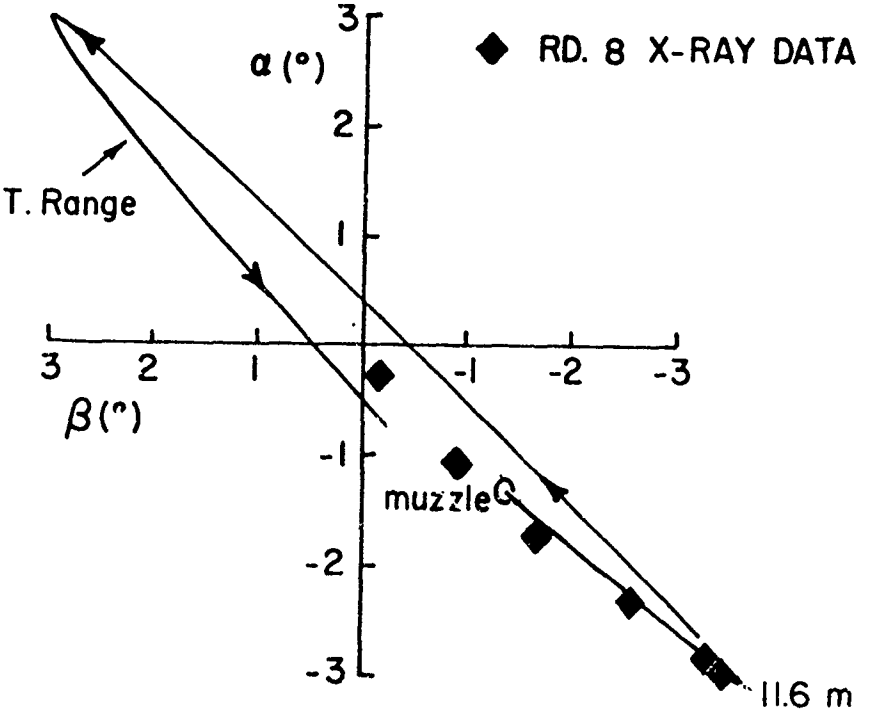

Figure 13. Comparison of Transonic Range and X-Ray Data, Round 8

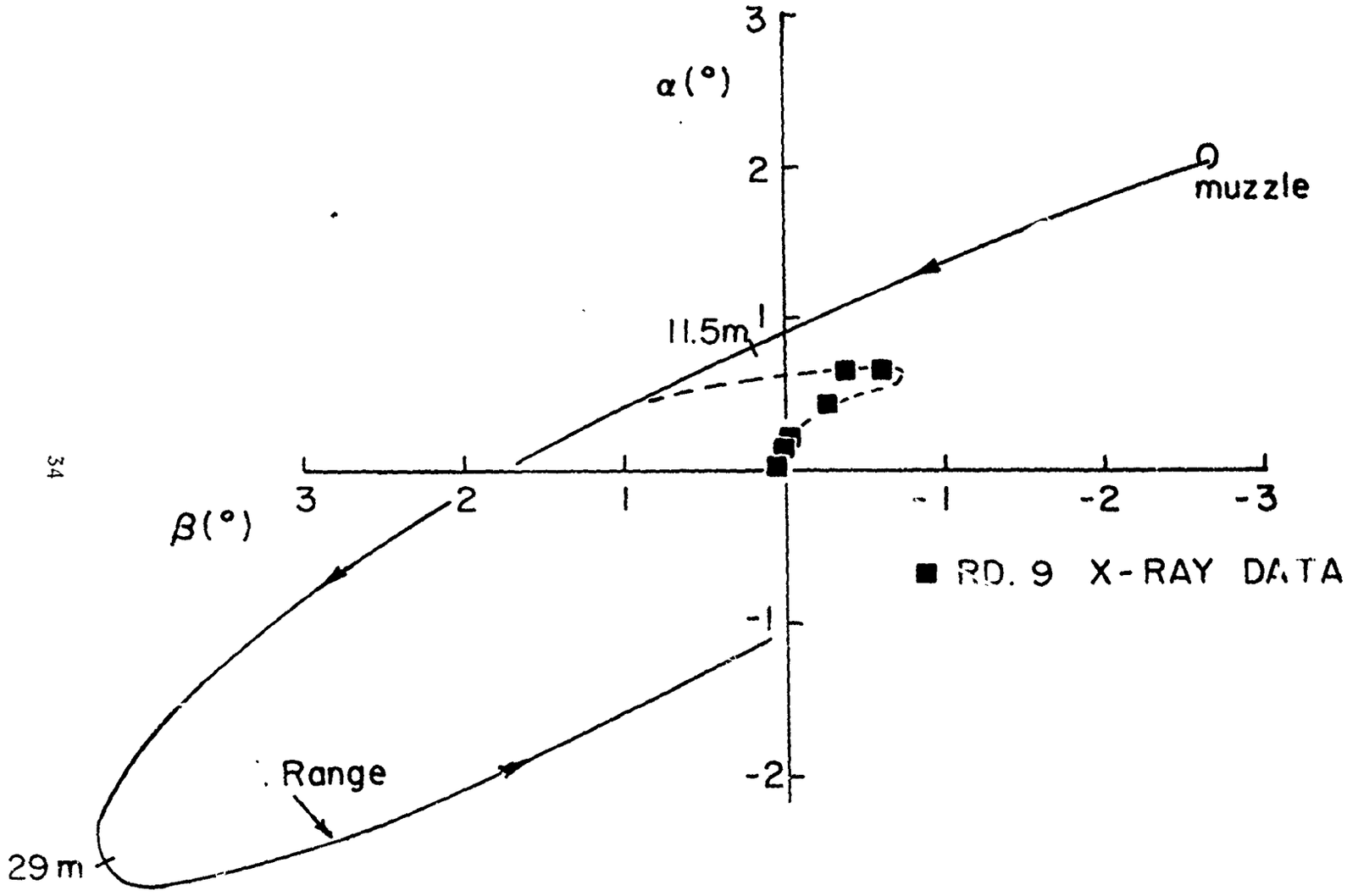

Figure 14. Comparison of Transonic Range and X-Ray Data, Round 9

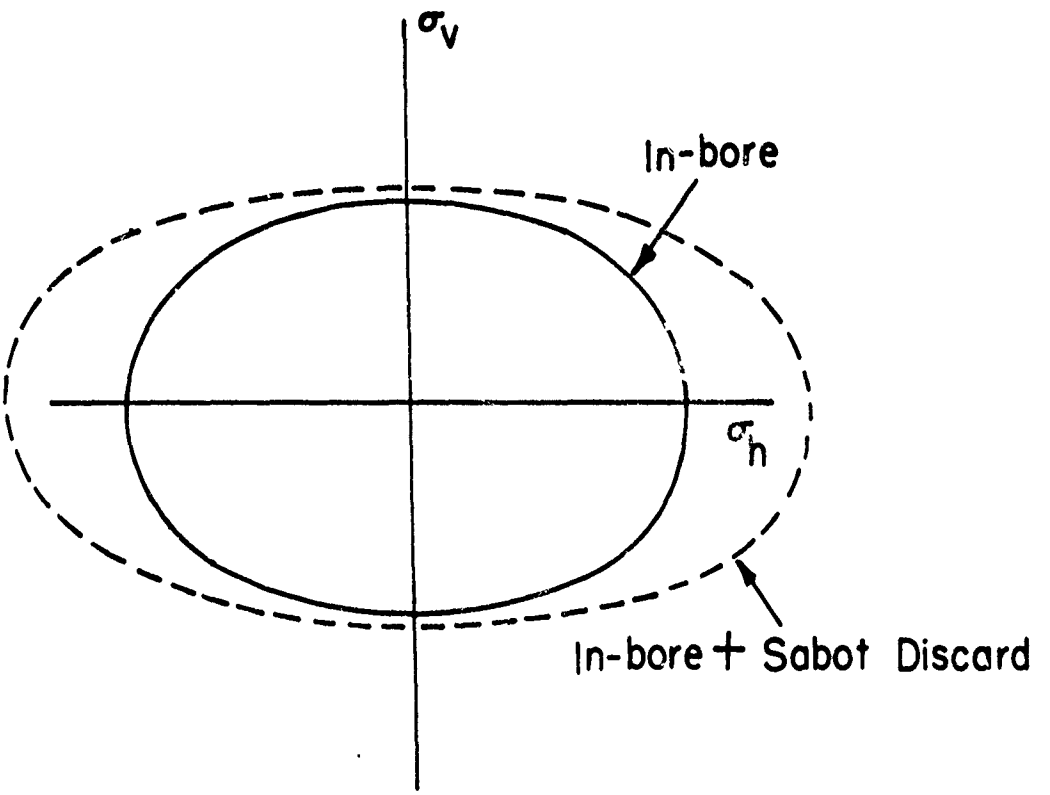

Figure 15. Relative Amplification of Dispersion

REFERENCES

1. Sears, W. R., ed., "Aerodynamic Interference," AGARD, CP-71-71, January 1971.

2. Gallagher, W. J., "Elements which have Contributed to Dispersion in the 90/40mm Projectile," Ballistic Research Laboratory Report No. 1013, March 1957, AD 135306.

3. Conn, H., "The Influence of Sabot Separation on the Yawing Motion of a Cone," Defense Research Establishment, Valcartier, Canada. TN 1849/70, June 1970, AD 880697L.

4. Glauz, W. D., "Estimation of Forces on a Flechette Resulting from a Shock Wave," Midwest Research Institute, Kansas City, MO, Final Report 19 June 1970 - 18 March 1971, May 1971. AD 724178.

5. Gretler, W., "Intermediate Ballistics Investigations of Wing Stabilized Projectiles," Deutschen, Versuchsanstaldt fur Luft-und Raumfahrt, Aachen, Germany, R67-92, November 1967.

6. Schmidt, E. M., Fansler, K. S., and Shear, D. D., "Trajectory Perturbations of Fin-Stabilized Projectiles due to Muzzle Blast," Journal of Spacecraft and Rockets, Vol 14, June 1977, pp. 339-344.

7. Schmidt, E. M. and Shear, D. D., "Launch Dynamics of a Single Flechette Round," Ballistic Research Laboratory Report No. 1810, August 1975, AD B006781L.

8. Ames Research Staff, "Equations, Tables, and Charts for Compressible Flow," NACA 1135, 1953.

LIST OF SYMBOLS

A	cross section area of projectile
C_D, C_{L_α}, C_{M_α}	drag, lift and pitching moment coefficients
I_x, I_y	axial and transverse projectile moments of inertia
L	period of yaw
ℓ	diameter of projectile
M	Mach number, or moment
p_∞, p_2, p_{t_3}	ambient pressure, pressure behind oblique shock, and pressure on fin surfaces due to oblique shock reflection
V	projectile velocity
x,y,z	orthogonal coordinate system (z is directed downrange)
α, β	projectile angle of attack and sideslip
ξ	complex angle of yaw
ρ	air density

Subscripts

o	conditions at entry into undisturbed free flight
2	conditions at X-ray station number 2

DISTRIBUTION LIST

No. of Copies	Organization
12	Commander Defense Documentation Center ATTN: DDC-TCA Cameron Station Alexandria, VA 22314
1	Director Defense Nuclear Agency Washington, DC 20305
1	Commander US Army Materiel Development and Readiness Command ATTN: DRCDMA-ST 5001 Eisenhower Avenue Alexandria, VA 22333
1	Commander US Army Materiel Development and Readiness Command ATTN: DRCDL 5001 Eisenhower Avenue Alexandria, VA 22333
3	Commander US Army Aviation Research and Development Command ATTN: DRSAV-E DRSAV-EQA, CPT Schrage DRCPM-AAH, M.Corgiatt 12th and Spruce Streets St. Louis, MO 63166
1	Director US Army Air Mobility Research and Development Laboratory Ames Research Center Moffett Field, CA 94035
1	Commander US Army Electronics Command ATTN: DRSEL-RD Fort Monmouth, NJ 07703
1	Commander US Army Jefferson Proving Ground ATTN: STEJP-TD-D Madison, IN 47250
4	Commander US Army Missile Research and Development Command ATTN: DRDMI-R DRDMI-RBL DRDMI-RDK Mr. R. Becht Mr. R. Deep Redstone Arsenal, AL 35809
1	Commander US Army Tank Automotive Development Command ATTN: DRDTA-RWL Warren, MI 48090
2	Commander US Army Mobility Equipment Research & Development Command ATTN: Tech Docu Cen, Bldg. 315 DRSME-RZT Fort Belvoir, VA 22060
5	Commander US Army Armament Materiel Readiness Command ATTN: Technical Lib DRSAR-RDG, J. Blick Rock Island, IL 61202
7	Commander US Army Armament Research and Development Command ATTN: DRDAR-TDS, Mr. Lindner DRDAR-LC-F, Mr.A.Loeb Mr. E. Friedman DRDAR-LCV, Mr. Barrieres Mr. R. Reisman DRDAR-SCW, Mr. Townsend DRDAR-SCN, Mr. Kahn Dover, NJ 07801

Preceding Page Blan

DISTRIBUTION LIST

No. of Copies	Organization
1	Commander US Army Armament Research and Development Command ATTN: PM, XM788/789 LTC Delany Dover, NJ 07801
4	Commander US Army Watervliet Arsenal ATTN: Tech Lib DRDAR-LCB, Dr.F.Sautter Dr. G. Carofano Mr. P. Alto Watervliet, NY 12189
2	Commander US Army Harry Diamond Labs ATTN: DRXDO-TI DRXDO-DAB, H.J. Davis 2800 Powder Mill Road Adelphi, MD 20783
1	Commander US Army Materials and Mechanics Research Center ATTN: DRXMR-ATL Watertown, MA 02172
1	Commander US Army Natick Research and Development Command ATTN: DRXRE, Dr. D. Sieling Natick, MA 01762
1	Director US Army TRADOC Systems Analysis Activity ATTN: ATAA-SL (Tech Lib) White Sands Missile Range NM 88002
1	Commander US Army Research Office ATTN: CRD-AA-EH P. O. Box 12211 Research Triangle Park NC 27709

No. of Copies	Organization
1	Director US Army BMD Advanced Technology Center P. O. Box 1500, West Station Huntsville, AL 35807
1	Commander US Army Ballistic Missile Defense Systems Command Huntsville, AL 35804
1	Director US Army Advanced Materiel Concepts Agency 5001 Eisenhower Avenue Alexandria, VA 22333
3	Commander US Naval Air Systems Command ATTN: AIR-604 Washington, DC 20360
3	Commander US Naval Ordnance Systems Command ATTN: ORD-9132 Washington, DC 20360
2	Commander and Director David W. Taylor Naval Ship Research and Development Center ATTN: Tech Lib Aerodynamic Lab Bethesda, MD 20084
3	Commander US Naval Surface Weapons Ctr ATTN: Code 6X Mr. F. H. Maille Dr. J. Yagla Dr. G. Moore Dahlgren, VA 22448

DISTRIBUTION LIST

No. of Copies	Organization
2	Commander US Naval Surface Weapons Ctr ATTN: Code 312, Mr. F. Regan Code 730, Tech Lib Silver Spring, MD 20910
1	Commander US Naval Weapons Center ATTN: Code 553, Tech Lib China Lake, CA 93555
3	Commander US Naval Research Laboratory ATTN: Tech Info Div Code 7700, D.A. Kolb Code 7720, Dr.E.McClean Washington, DC 20375
1	Commander US Naval Ordnance Station ATTN: Code FS13A, P.Sewell Indian Head, MD 20640
1	AFRPL/LKCB, Dr. Horning Edwards AFB, CA 93523
2	AFATL (DLRA, F. Burgess; Tech Lib) Eglin AFB, FL 32542
1	AFWL/DEV Kirtland AFB, NM 87117
1	ASD/XRA (Stinfo) Wright-Patterson AFB, OH 45433
1	Director National Aeronautics and Space Administration George C. Marshall Space Flight Center ATTN: MS-I, Lib Huntsville, AL 35812
1	Director Jet Propulsion Laboratory ATTN: Tech Lib 2800 Oak Grove Drive Pasadena, CA 91103
1	Director National Aeronautics and Space Administration Langley Research Center ATTN: MS 185, Tech Lib Langley Station Hampton, VA 23365
1	Director NASA Scientific & Technical Information Facility ATTN: SAK/DL P. O. Box 8757 Baltimore/Washington International Airport, MD 21240
1	AAI Corporation ATTN: Dr. T. Stastny Cockeysville, MD 21030
1	Advanced Technology Labs ATTN: Dr. J. Erdos Merrick & Stewart Avenues Westbury, NY 11590
1	Aerospace Corporation ATTN: Dr. T. Taylor P. O. Box 92957 Los Angeles, CA 90009
1	ARO, Inc. ATTN: Tech Lib Arnold AFS, TN 37389
1	ARO, Inc. Von Karman Gasdynamics Facility ATTN: Dr. J. Adams Arnold AFS, TN 37389

DISTRIBUTION LIST

No. of Copies	Organization
1	ARTEC Associates, Inc. ATTN: Dr. S. Gill 26046 Eden Landing Road Hayward, CA 94545
1	AVCO Systems Division ATTN: Dr. W. Reinecke 201 Lowell Street Wilmington, MA 01887
1	Battelle Columbus Labs ATTN: J. E. Backofen, Jr. 505 King Avenue Columbus, OH 43201
1	Technical Director Colt Firearms Corporation 150 Huyshore Avenue Hartford, CT 14061
2	General Electric Corporation Armaments Division ATTN: Mr. R. Whyte Mr. J. MacNeil Lakeside Avenue Burlington, VT 05401
1	Honeywell, Inc. ATTN: Mail Station MN 112190 G. Stilley 600 Second Street, North Hopkins, MN 55343
1	Martin Marietta Aerospace ATTN: Mr. A. J. Culotta P. O. Box 5387 Orlando, FL 32805
1	Winchester-Western Division Olin Corporation New Haven, CT 06504
1	Rockwell Int Science Center ATTN: Dr. Norman Malmuth P. O. Box 1085 1000 Oaks, CA 91360
1	Sandia Laboratories ATTN: Aerodynamics Dept Org 5620, R. Maydew Albuquerque, NM 87115
1	S&D Dynamics, Inc. ATTN: Dr. M. Soifer 755 New York Avenue Huntington, NY 11743
1	Guggenheim Aeronautical Lab California Institute of Tech ATTN: Tech Lib Pasadena, CA 91104
1	Franklin Institute ATTN: Tech Lib Race & 20th Streets Philadelphia, PA 19103
1	Director Applied Physics Laboratory The Johns Hopkins University Johns Hopkins Road Laurel, MD 20810
1	Massachusetts Institute of Technology Dept of Aeronautics and Astronautics ATTN: Tech Lib 77 Massachusetts Avenue Cambridge, MA 02139
1	Ohio State University Dept of Aeronautics and Astronautical Engineering ATTN: Tech Lib Columbus, OH 43210

DISTRIBUTION LIST

No. of Copies	Organization
2	Polytechnic Institute of New York Graduate Center ATTN: Tech Lib Dr. G. Moretti Route 110 Farmingdale, NY 11735
1	Director Forrestal Research Center Princeton University Princeton, NJ 08540
1	Forrestal Campus Library Princeton University ATTN: Dr. M. Summerfield P. O. Box 710 Princeton, NJ 08540
1	Southwest Research Institute ATTN: Mr. Peter S. Westine P. O. Drawer 28510 8500 Culebra Road San Antonio, TX 78228
	Aberdeen Proving Ground
	Marine Corps Ln Ofc Dir, USAMSAA Cdr, USACSL/EA ATTN: DRDAR-ACW, A.Flatau Bldg. E3516